Comparative micro computed tomography study of a vertebral body

Susanne Drews[a,b], Felix Beckmann[c], Julia Herzen[c], Oliver Brunke[d], Phil Salmon[e], Sebastian Friess[f], Andres Laib[g], Bruno Koller[g], Thomas Hemberger[d] Magdalena Müller-Gerbl[a] and Bert Müller*[h]
[a]Institute of Anatomy, University of Basel, 4056 Basel, SWITZERLAND;
[b]Kantonsspital Bruderholz, 4101 Bruderholz, SWITZERLAND;
[c]GKSS-Research Center, 21502 Geesthacht, GERMANY;
[d]phoenix|x-ray Systems + Services GmbH, 31515 Wunstorf, GERMANY;
[e]Skyscan, 2550 Kontich, BELGIUM;
[f]Gloor Instruments AG, 8610 Uster, SWITZERLAND;
[g]Scanco Medical AG, 8306 Brütisellen, SWITZERLAND;
[h]Biomaterials Science Center, University of Basel, 4031 Basel, SWITZERLAND

ABSTRACT

Investigations of bony tissues are often performed using micro computed tomography based on X-rays, since the calcium distribution leads to superior contrast. Osteoporotic bone, for example, can be well compared with healthy one with respect to density and morphology. Degenerative and rheumatoid diseases usually start, however, at the bone-cartilage-interface, which is hardly accessible. The direct influence on the bone itself becomes only visible at later stage. For the development of suitable therapies against degenerative cartilage damages the exact three-dimensional description of the bone-cartilage interface is vital, as demonstrated for transplanted cartilage-cells or bone-cartilage-constructs in animal models. So far, the morphological characterization was restricted to magnetic resonance imaging (MRI) with poor spatial resolution or to time-consuming histological sectioning with appropriate spatial resolution only in two rather arbitrarily chosen directions. Therefore, one should develop μCT to extract the features of low absorbing cartilage. The morphology and the volume of the inter-vertebral cartilage disc of lumbar motion segments have been determined for one PMMA embedded specimen. Tomograms were recorded using nanotom® (Phoenix|x-ray, Wunstorf, Germany), μCT 35™ (Scanco Medical, Brütisellen, Switzerland), 1172™ and 1174™ (both Skyscan, Kontich, Belgium), as well as using the SRμCT at HASYLAB/DESY. Conventional and SRμCT can provide the morphology and the volume of cartilage between bones. Increasing the acquisition time, the signal-to-noise ratio becomes better and better but the prominent artifacts in conventional μCT as the result of inhomogeneously distributed bony tissue prevents the exact segmentation of cartilage. SRμCT allows segmenting the cartilage but requires long periods of expensive beam-time to obtain reasonable contrast.

Keywords: spine, bone-cartilage interface, synchrotron radiation, micro computed tomography

1. INTRODUCTION

In the last decades low back pain is becoming into the focus of public attention. Public opinion polls showed that more than 70% of people suffered from acute low back pain at least once. Approximately 5% have chronic low back pain, which is defined as low back pain lasting for more than 3 months.[1] Economic damage for western nations caused by loss of working hours and medical costs is immense.[2,3] There are different reasons for chronic low back pain according to gender, age and grade of activity. The specific chronic low back pain includes infections, tumors, osteoporosis, ankylosing spondylitis, fractures, deformities and inflammatory processes but for a large group no pathological correlation has been found.[4] Because the problem of low back pain will increase with the population getting older, the role of the morphology of the physiologic and pathologic spine will become more and more important. Especially for the description of bone morphology μCT established as appropriate method.[5] It allows showing changes of the trabecular bone non-destructively. Advanced μCT-systems permit a nominal micrometer resolution, sometimes even voxel sizes smaller than 1 μm. Nevertheless, diseases discussed in context with low back pain often concern the inter-vertebral disc consisting of anisotropic cartilage. Diseases such as rheumatoid arthritis and arthrosis have generally their origin at the bone-cartilage interface. In contrast to bone, cartilage is poorly x-ray absorbing and therefore hardly accessible for CT

Developments in X-Ray Tomography VI, edited by Stuart R. Stock,
Proc. of SPIE Vol. 7078, 70780C, (2008) · 0277-786X/08/$18 · doi: 10.1117/12.793815

analysis. Other modalities that make visible soft tissue, for example magnet resonance imaging (MRI), still lack of spatial resolution. The traditional method of histological sectioning is time consuming and results in significantly reduced resolution in one direction. Furthermore, it is destructive so that further examination is restricted. The objective of this study has been the simultaneous visualization of bone and cartilage. For that, we compared the results of four different µCT systems. One has to figure out, which system allows visualizing the cartilage tissue. This is expected to be mainly a result of the density resolution (contrast), often characterized by the full width at half maximum (FWHM) in the absorption value histogram.[6] A detailed histogram analysis of the identical volume could indicate the µCT-system performance in quantitative manner. At the first glance, the SRµCT based on monochromatic x-rays should provide the best performance. Because of the restricted availability, however, more or less advanced conventional µCT systems are developed to powerfully analyze bony tissue. The direct comparison of conventional with SR-based µCT is therefore desired, especially to elucidate the strengths and potential weaknesses of different systems available on the market.

2. MATERIAL AND METHODS

2.1 Preparation of the motion segment

The juvenile human motion segment studied consisted of two vertebral bodies, the inter-vertebral disc and the anterior and posterior longitudinal ligament. The vertebral arch was cut off using a band saw. It was harvested out of the lumbar region, embedded in PMMA. This PMMA embedding is a common method for conventional histology. It still contains the trabecular structure and makes possible long-term storage as solid state. The embedded samples were cut into four quarters. One of these quarters, which had a maximal diameter of 1.3 cm was measured at the selected facilities to extract the micro-morphology of the bone including surrounding soft tissues.

2.2 Synchrotron radiation-based µCT measurements

The SRµCT measurements were carried out in the absorption contrast mode at the beamline W 2,[7] operated by the GKSS Research Center, using the photon energy of 28 keV. The spatial resolution determined by the modulation transfer function at a metallic edge[8] corresponded to 13.9 µm at a pixel size of 6.8 µm. The projections were recorded with an asymmetric rotation axis and 360° rotation to increase the spatial resolution almost by a factor of two with respect to 180° rotation regularly used for parallel x-rays.[9] For the reconstruction by means of the filtered back-projection algorithm[10] two out of the 1441 projections were combined. To obtain the 3D dataset of the region of interest, four tomograms shifted by 2.3 mm each were manually registered with pixel size resolution.

2.3 Micro computed tomography measurements

The µCT measurements were performed with four systems of three manufacturers: nanotom® (Phoenix|x-ray, Wunstorf, Germany), µCT 35™ (Scanco Medical, Brütisellen, Switzerland), 1172™ and 1174™ (both Skyscan, Kontich, Belgium).

2.3.1 Measurements using nanotom®

In 2006, phoenix|x-ray introduced a flexible, high-resolution laboratory CT system for applications in fields such as materials science, micro-mechanics, electronics, geology, and biology. The nanotom® is equipped with an in-house developed 180 kV high-power nanofocus® x-ray tube. This source offers different operation modes. For examinations of small and/or low absorbing samples the nanofocus® mode is applied. Here, the tube can reach an emission spot smaller than 0.8 µm, which is necessary to obtain sharp features at sub-micrometer voxel-sizes. For larger samples (up to 120 mm in diameter and maximal weight of 1 kg) or highly absorbing materials such as steel or copper, the tube operates in the high-power mode (up to 15 W target power). The flat panel detector consisting of 50 µm-wide pixels (active area 120 mm x 120 mm, 2300 x 2300 pixels) is extended 360 mm detection width by means of three positions. To minimize the influences of vibrations or thermal expansion, the essential parts namely tube, detector and rotation unit are mounted on a high-precision, granite-based manipulation system. To guarantee stability for long-term measurements, dedicated materials and refined designs including air-bearing of the rotation unit are incorporated. Therefore, it is particularly suitable for examination and measurement of molded parts, sensors, complex mechatronic samples, microelectronic components as well as for material samples such as synthetic materials, metals, ceramics, sintered alloys, composite materials, mineral and organic samples.

2.3.2 Measurements using µCT 35™

The µCT 35™ is a high-resolution desktop cone beam scanner. It is equipped with a microfocus x-ray source, which acceleration voltage is adjustable between 30 and 70 kV with a beam current of 160 µA. The detector consists of 2048 x 128 pixels (image matrix 4096 x 4096 pixels). Depending on the sample diameter, one achieves a spatial resolution of less than 5 µm determined by the 10% threshold of the modulated transfer function. The specimens of interest with a diameter up to 36 mm and a height of up to 140 mm are placed inside the cylindrical sample holder and fixated by means of low absorbing solid polymer foam. This guarantees perfect sample alignment. The typical scan takes 3 to 14 s per slice. The system is designed for quantitative bone analysis. After bone density calibration it works automatically. The batch mode allows large object or multiple object scanning. The settings, i.e. spatial resolution, photon energy, etc. can be set for each scans in one batch, individually. It should be noted that each scan is related to individually selected bright or dark-field correction, which is necessary to optimize the scanning time. The 3D evaluation is integrated into the scanning computer system. Hence, no time-consuming data transfer between computers or programs is necessary for the different steps of the procedure, i.e. between scanning, reconstruction and data analysis.

2.3.3 Measurements using 1174™ and 1172™

The rotation stage allow for secure and precise sample positioning. The accelerating voltage of the x-ray microfocus source and the filter were selected to obtain an optimized total x-ray absorption in the projection of the specimen of interest. Low x-ray absorption results in excessive image noise. For homogenous samples, Grodzins[11] derived the optimal values for the photon energies. The reconstruction was performed with a modified Feldkamp algorithm[12] using Skyscan Nrecon™ software[13] on a cluster of four PCs. The SkyScan 1172™ and 1174™ desktop micro-CT scanners represent different levels of µCT imaging performance. The 1174™ is a portable instrument with simplified design, notably a fixed sample rotation stage with variable magnification achieved by focus adjustment between x-ray scintillator and CCD detector. In the 1172™ high-resolution desktop scanner, magnification is realized in the conventional way by moving the sample in-line between source and detector. This mode necessitates a spot size of 5 µm to allow for micrometer resolution at high magnifications. Static sample stages as realized in the 1174™ system reduce such a requirement and permit large spot sizes associated with high x-ray power and short acquisition times. The high x-ray power allows employing a thin x-ray scintillator, which enhances the spatial resolution of the system. Note that in the 1172™ scanner, the reduced detection efficiency related to the greater source-detector distance needed for variable sample positioning is significantly mitigated by optimizing the sample position for given magnification.

2.4 Summary of the scanning parameters

Based on visual on-side inspection of the embedded vertebral body, the manufacturers selected the parameters for the µCT measurements. Table 1 summarizes the selected parameters for both data acquisition and reconstruction.

Table 1. Scanning and reconstruction parameters of the µCT-measurements at the different facilities.

Instrument	Phoenix|x-ray Nanotom®	Scanco Medical µCT 35™	SkyScan 1174™ µCT	SkyScan 1172™ µCT	HASYLAB/DESY SRµCT
Scanning					
Focus object distance [mm]	44	116	181	95	
Focus detector distance [mm]	220	271	225	217	
Voxel size [µm]	10	10	20	10	6.8
Acceleration voltage [kV]	80	70	50	70	(28 keV)
Beam current [µA]	180	114	800	141	

Focal spot diameter [µm]	3	7			
Filter inserted	none	0.5 mm Al + 0.13 mm Be	0.5 mm Al	0.7 mm Al	Double crystal
Specimen rotation	360°	360°	180°	180°	360°
Rotation step	0.3°	0.18°	0.4°	0.25°	0.25°
Integration time [s]	0.5	2x0.55			
Frame averaging	5	2	3	4	
Scan duration [min]	80	2x56	63	45.5	4x195
Reconstruction					
Beam hardening correction, [%]	Yes (4)	Specialized for bone density	30	30	None
Ring artifact compensation	Yes	Yes	16	15	None
Smoothing	No	No	1	1	None

2.5 Pre-registration of the µCT with the SRµCT data

In order to compare the different µCT-systems, the common volume of the sample has to be extracted. For the purpose, the data of the vertebral body were manually pre-registered and finally registered using the dedicated computer code in an automatic fashion.

In the first step the data were binned to obtain comparable voxel sizes for the differently acquired tomograms. Based on the voxel sizes shown in Table 1, the following binning factors were chosen: nanotom®, µCT 35™ and 1172™ a factor of four, 1174™ a factor of two, and SRµCT a factor of six. The binning leads to much smaller datasets, which allow easier processing. Furthermore, the binning gives rise to improved density resolution or contrast.[6]

In the second step, the µCT-data were interactively registered with the SRµCT-data. Based on a rather simple IDL code the data were represented by slices in the three orthogonal directions as demonstrated in Figure 1. The user should select three non-collinear anatomical landmarks in both datasets that form two planes for the coordination transform. Subsequently, the µCT-data were translated, rotated and scaled to obtain the reasonable estimate for the automatic registration procedure. The tool also helps to visualize the three slices to validate the pre-registration procedure.

2.6 Processing of the absorption value histograms

Density resolution is represented by the histogram of the local absorption values of the entire tomograms. A quantitative parameter is the full width at half maximum (FWHM) of the peaks of interest. For SRµCT, one usually observes peaks with the characteristic Gaussian shape.[8] In the present study, the peaks of all histograms show more or less the Gaussian shape. Therefore, the experimental data were fitted by means of the ProFit code (ProFit 6.0.6, Quantumsoft, Zurich, Switzerland) based on the Levenberg-Marquardt algorithm.

Because of the different energy spectra of the µCT systems, a direct quantitative comparison appears impossible. One might assume, however, that the main peaks are somehow characteristic and their FWHM can be correlated with their separation. Consequently, the absorption values can be scaled according to this separation for the semi-quantitative comparison of the density resolution of the µCT systems for the selected vertebral body specimen.

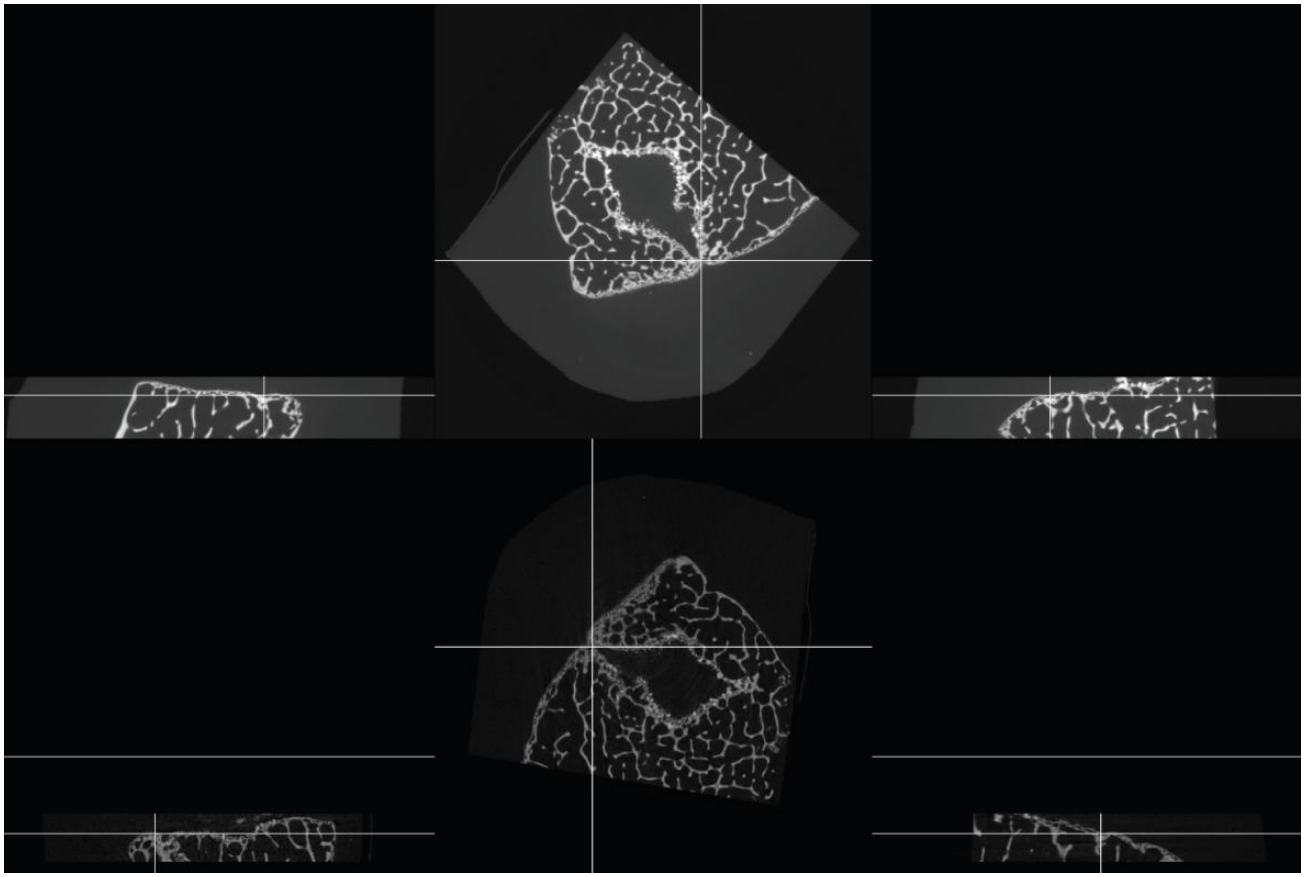

Fig. 1. The vertebral body is represented by slices in the three orthogonal directions for pre-registration of the SRμCT-data (top) with the other μCT-dataset (below). For each modality, one selects three corresponding landmarks, which define the transform for pre-registration.

3. RESULTS

3.1 Determination of the common volume

In order to extract the common volume of the different tomographic data, the μCT data have to be registered with the SRμCT data by means of an affine transformation. The algorithm based on the rigid matching uses the classical maximization of the mutual information principle.[14, 15] The nine registration parameters, three for each translation, rotation and scaling are found using the Powell multi-dimensional search algorithm[16] such that the mutual information between the SRμCT-reference and the μCT-data is maximized. By means of the pre-registered data, which showed to represent reasonable estimates, a high degree of conformity is reached, implying that significant distortions between the systems can be excluded. Figure 2 demonstrates this conformity for one selected slice of each system, although individual artifacts and absorption value differences are clearly visible. Note, the paper partly glued onto the PMMA embedding exhibits different shapes, but does not significantly alter the result of registration.

The registered, binned 8-bit data permit the selection and the extraction of the common volume out of the original, high-resolution 16-bit tomograms. These data are the basis for the histogram analysis.

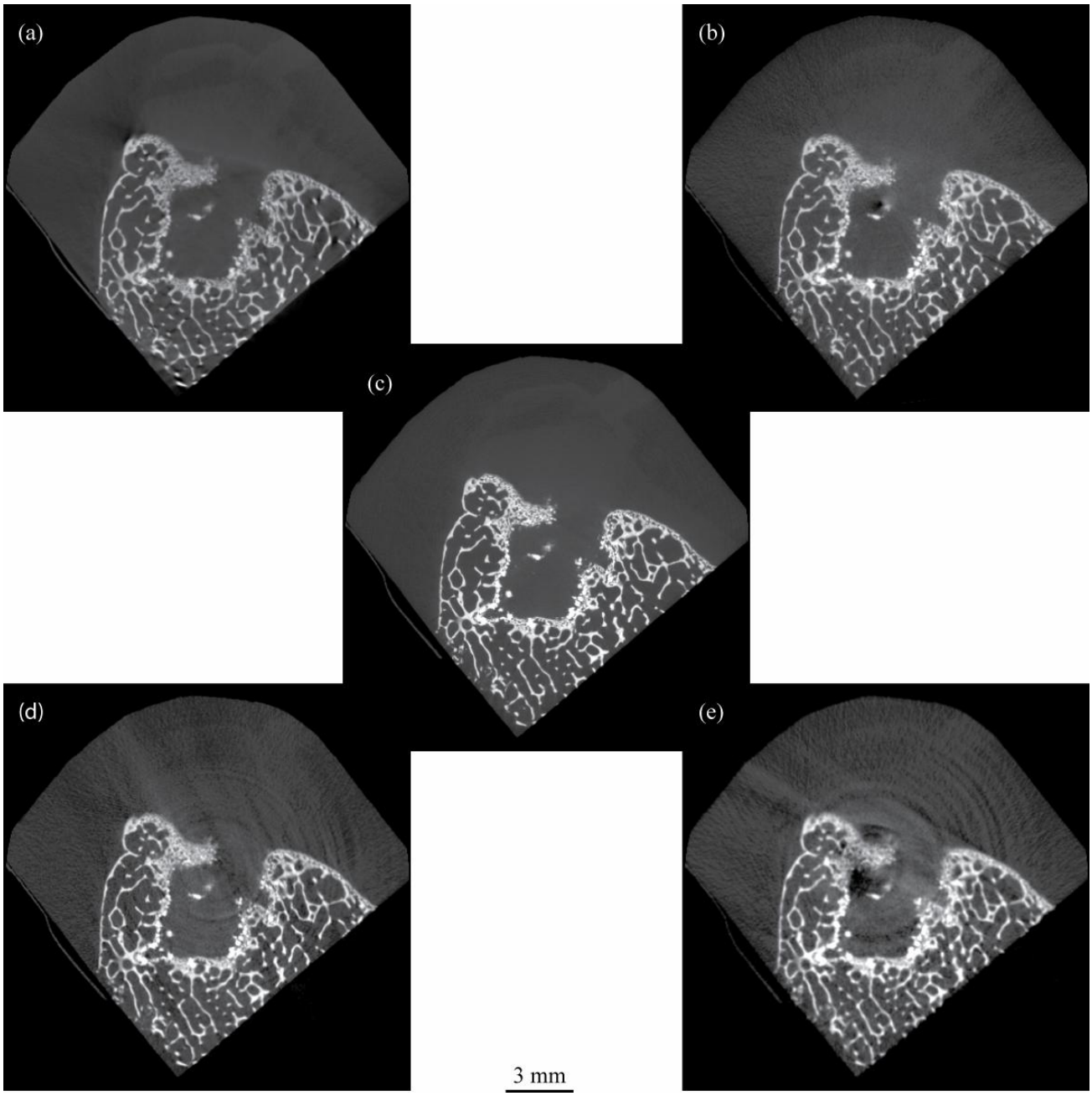

Fig. 2: CT slices of the identical region scaled according to the SRμCT absorption values from -0.11 to 2.40 cm^{-1}. The images are arranged in alphabetical order around (c) HASYLAB ((a) Phoenix | x-rays, (b) Scanco Medical, (d) Skyscan 1172, (e) Skyscan 1174).

3.2 Histogram analysis of the local absorption values

The histograms of the local absorption values provide a powerful approach to uncover the density resolution of tomography systems for the specimen under consideration. The histograms of the common volume allow for the direct comparison of the μCT-systems with the SRμCT-system, which takes advantage of monochromatic x-rays and is used here as the golden standard.

In Figure 3 the histograms of the local absorption coefficient for the four μCT-systems are shown in comparison to the reference SRμCT-dataset together with the related fits by means of three Gaussians for each histogram. The absorption

values given on the axis are only related to the SRμCT-data. The μCT histograms were prepared in the following manner. First, the positions of the two main peaks have been determined and have been shifted manually to the peaks of SRμCT-data. Second, the data have been reduced to obtain about 100 values between the peaks, i.e. to reach comparative frequency values. Third, the half widths (FWHM) of the three Gaussians obtained from the fitting procedures have been related to the peak separation and have been summarized in Table 2 together with the statistical error bars.

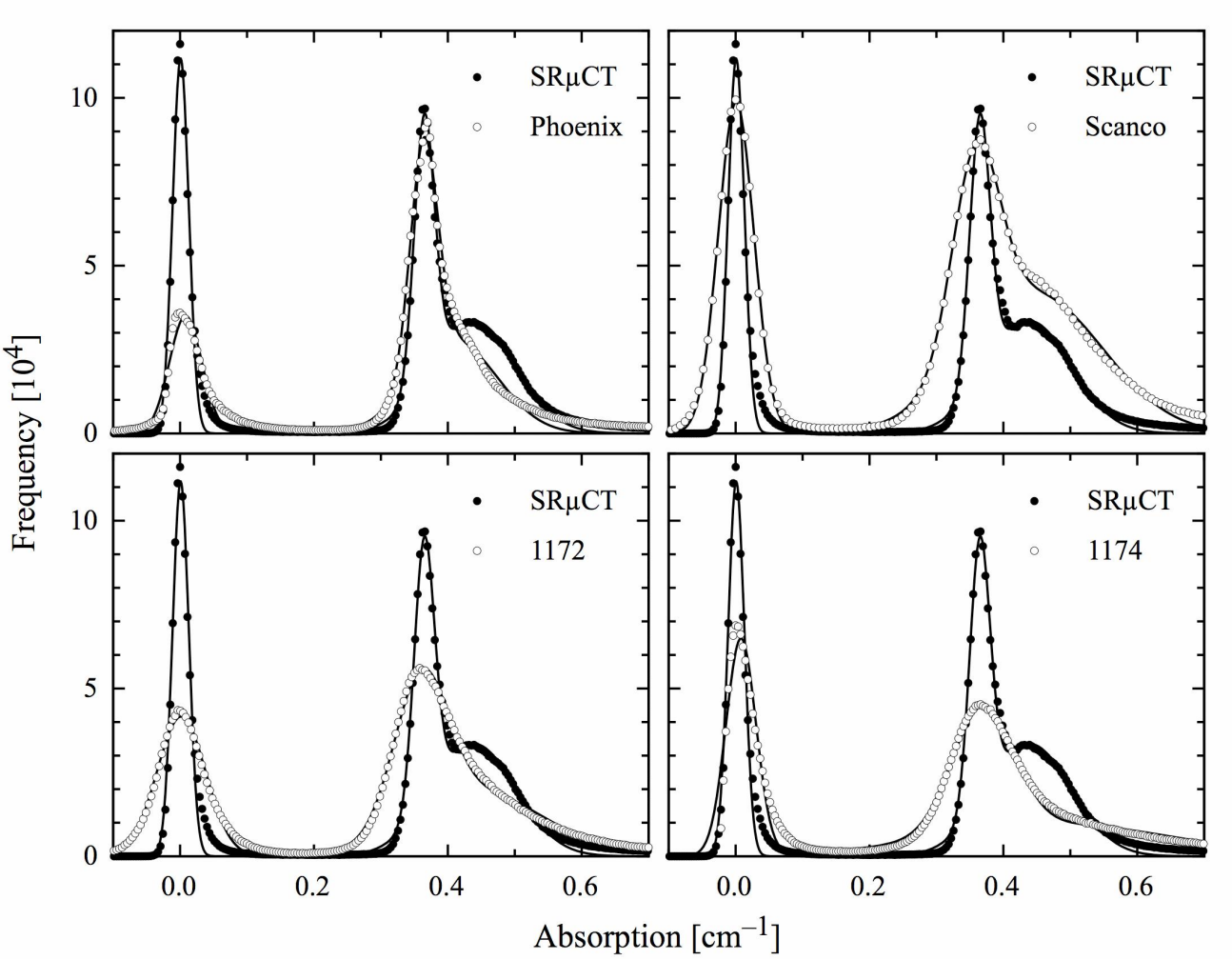

Fig. 3: The histograms of the gray values of the different μCT-systems are compared with the SRμCT histograms of the local absorption values. The peaks of the selected range were fitted by means of three Gaussians.

The fits using three Gaussians (fitting parameters: FWHM, position, and amplitude) describes the experimental data within the gray values of interest for the five experimental set-ups. The histograms allow determining the thresholds for identifying of the three components. Figure 4 demonstrates that the main peaks represent the air (blue-colored) and the embedding material (yellow). The embedded cartilage and soft tissue (red-colored) causes the shoulder for somehow larger absorption values than the pure embedding material, as shown in Figure 4 as well. The bony tissue (given in white) exhibits larger absorption values and is therefore not shown in the histograms of Figure 3.

Table 2. Half widths (FWHM) of Gaussians fitted to the histograms and related to the distance between main peaks [in %].

Instrument	FWHM air	FWHM embedding	FWHM soft tissue
SRμCT [%]	0.08±0.01	0.13±0.01	2.16±0.07
Phoenix X-ray [%]	0.33±0.01	0.23±0.01	2.31±0.07
Scanco Medical [%]	0.40±0.01	0.68±0.03	5.77±0.16
Skyscan 1172™ [%]	0.74±0.01	0.89±0.02	5.31±0.17
Skyscan 1174™ [%]	0.28±0.01	1.17±0.03	16.84±0.80

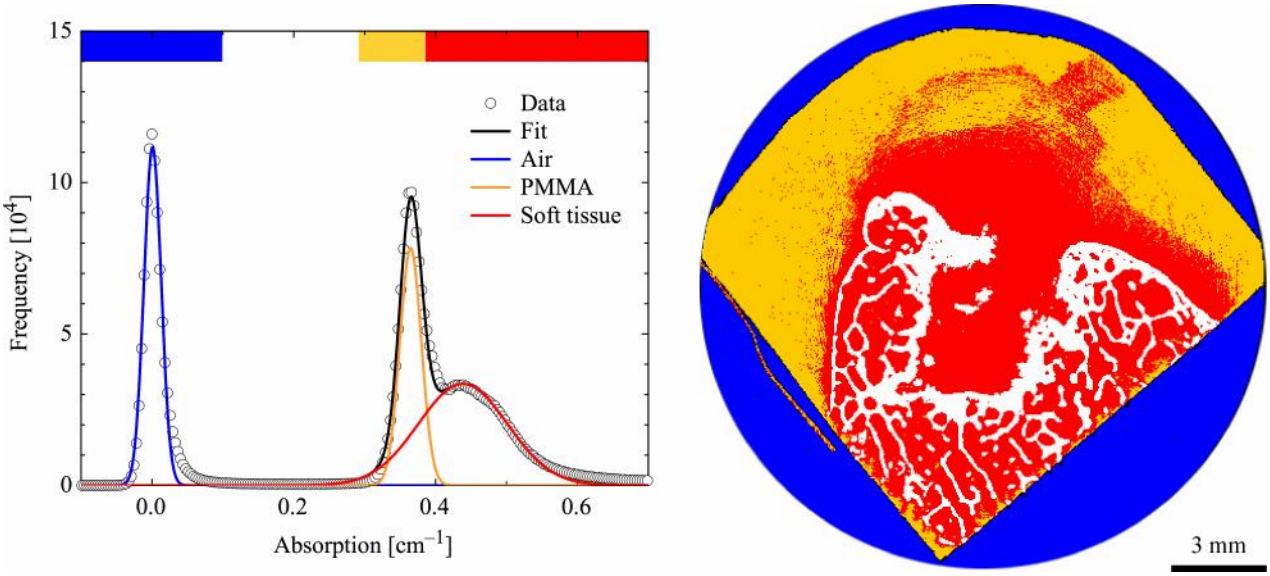

Fig. 4: Histogram of the SRμCT-data together with the fitted Gaussians (left) and one selected slice colored accordingly.

It has to be mentioned that the peak related to the air is smaller for the nanotom® and the Skyscan systems. This is due to the segmentation of the common volume that not only contains air but also a region outside the reconstructed volume. Therefore, this part is not really representative and might be regarded as artifact.

Comparing the nanotom® and the SRμCT histograms, one finds an astonishing quantitative agreement for embedding and soft tissue components. The shape of the peak associated with air, however, differs from the Gaussian. Its FWHM is a factor of four larger than that of the SRμCT-data.

The histogram of the μCT-system from Scanco Medical does not exhibit any visible distortion. The peaks are only broadened with respect to the SRμCT results associated with reduced density resolution, which is expected for the bremsstrahlung source. Nevertheless, it is of interest that the shoulder related to the embedded soft tissue including cartilage is properly present and much better represented than for the other μCT-systems.

The two systems from Skyscan yield comparable density resolution, but do hardly reach the contrast of the other μCT-systems. The ring-like artifacts, one recognizes in the slices of Figure 5, explain this behavior.

3.3 Description of selected tomographic slices

Figure 2 shows one slice from each μCT-system scaled as the histograms given in Figure 3. The gray-values were distributed between -0.11 and 2.40 cm^{-1} for the SRμCT-system. This choice is typical to visualize the bone with its trabecular structure and local variations of the bone density and degree of calcification. Figure 5 contains the same slices but scaled for optimized cartilage visualization, namely between 0.2 and 0.7 cm^{-1} (cp. Figure 3).

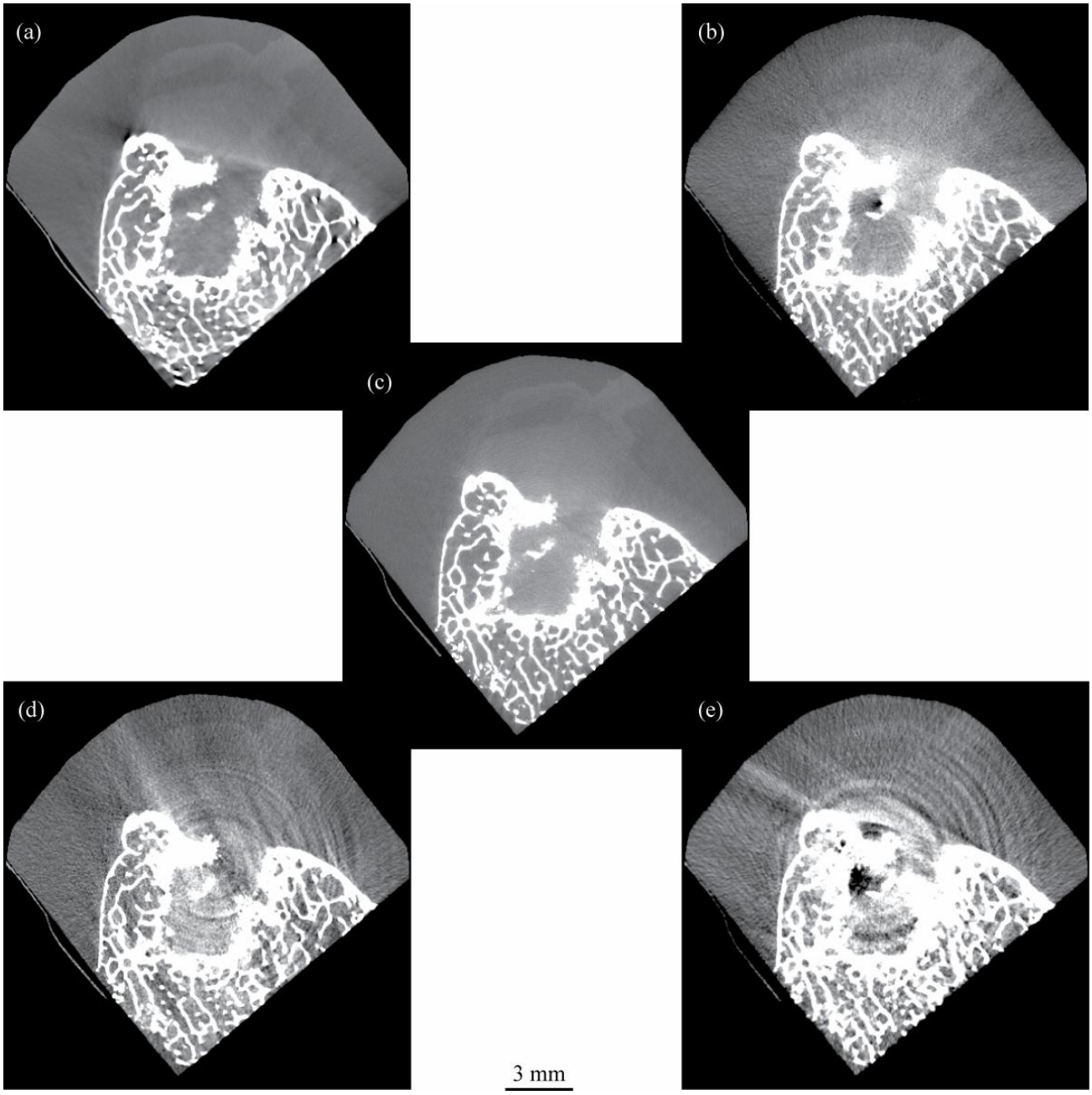

Fig. 5: µCT-slices of the identical region scaled according to the histograms in Figure 3 for absorption values from 0.2 to 0.7 cm^{-1}. The images are arranged in alphabetical order around (c) SRµCT, (a) Phoenix | x-rays, (b) Scanco Medical, (d) Skyscan 1172, (e) Skyscan 1174.

In the SRµCT-image in the center of Figure 2 one can identify the trabecular bone, the endplate, the PMMA embedding and to some extend the cartilage of the inter-vertebral disc. The vertebra's trabeculae shown in the lower edge exhibits regular sizing and typical homogeneous degree of calcification. The cut face of the vertebral endplate in the centre of the image is irregular. Here, several bright spots are present explained by small regions of higher degree of calcification. The PMMA embedding material shows the expected homogeneous x-ray absorption, which is higher than air but well below the bony tissue. Close to its x-ray absorption, one can see brighter irregularly shaped areas identified as cartilage and soft tissue. These embedded tissues appear isotropic. This means that the well-known cartilaginous structures such as annulus

fibrosus, nucleus pulposus and cartilaginous endplate cannot be distinguished. No signs of pathology regarding bone or cartilage degeneration could be identified.

The nanotom® yields a signal-to-noise ratio (S/N) comparable to the SRμCT-system. Bony as well as low absorbing cartilaginous tissues can be clearly distinguished from the PMMA embedding as seen in Figures 2 and 5. In Figure 2, also the differently calcified regions of the vertebral endplate become to light. Ring-like artifacts are effectively suppressed in the dataset. In the upper part on the left at the border between bone and PMMA a strong artifact is seen that could be a result of the beam-hardening and its correction. Such artifacts are also present within the spongy bone especially in the lower part of the image, where several black spots behind the trabeculae can be noticed.

The μCT 35 of Scanco Medical provides images that properly show the spongy bone and the differently calcified regions of the bony endplate. The distinction of cartilage and soft tissues from PMMA embedding is also possible, although the contrast obtained does not reach the quality of the SRμCT. Ring-like artifacts are effectively suppressed. There is quite a strong artifact in the center of the image that correlates with the reconstruction center. Such artifacts are only present at the lower and upper end of the stack and could be avoided by the use of larger overlaps between different stacks.

The Skyscan 1172 yields also reasonable results of the bony tissue. The differences in the degree of calcification are detectable. As already seen from the histograms, the images lack of contrast with respect to the SRμCT-data. The cartilage can hardly be detected and not segmented from the pure PMMA embedding. Note the artifacts represented by the streaks running from the bony edge diagonally upwards and are even clearer in Figure 5. Finally, the suppression of ring-like artifacts is not fully satisfying.

The rather simple Skyscann 1174 shows impressive performance, although the signal-to-noise ratio is the lowest one of the systems used. The images as shown in Figure 2 reproduce the bony tissue well and even show the differences in the degree of calcification. The contrast in the images, however, is too weak to characterize the embedded low absorbing cartilage and soft tissues. One might see features related to these tissues, but they are overlapped mainly from the ring-like artifacts. In addition, one finds streak artifacts and a major artifact located in the reconstruction center (cp. Figure 5).

3.4 Morphometric analysis of the trabecular bone

The analysis software of the μCT systems of Scanco Medical and of Skyscan offer the morphometric evaluation of the trabecular bone.

The software of Scanco Medical permits the determination of quantities as the bone volume density (BV/TV), which measures the volume of the bone trabeculae relative to the total volume, and the trabecular number (Tb.N) directly out of the pre-defined volume of interest (VOI). Based on these quantities further parameters such as trabecular thickness (Tb.Th) and trabecular separation are derived.[17] The left image of Figure 6 represents the Tb.Th in a 3D model of the common tomographic volume. The degree of anisotropy is calculated by means of the mean intercept length (MIL),[18] the average distance between two bone-marrow interfaces. By fitting the MIL-values to an ellipsoid, the degree of anisotropy can be defined.[17] Further Hildebrand and Rüegsegger[19] established the structure model index (SMI) a parameter describing trabeculae's shape as plate-like and rod-like.

The software of Skyscan allows calculating 3D and 2D morphometric parameters for the trabecular and cortical bone of the selected region of interest (ROI). Single gray value thresholds (68 and 120) were applied for the trabecular and cortical ROIs, respectively. The lower density threshold for trabecular bone allows segmentation of the finer structures. The thicker cortical bone can have higher threshold to more accurately represent thickness and porosity. The signal-to-noise ratios of the reconstructed images were high so that further image processing on the binarized images as despeckling were not likely to significantly improve measurement precision. The 3D parameters were based on analysis of a Marching Cubes[20] type model with a rendered surface. Calculations of 2D areas and perimeters were based on the Pratt algorithm.[21] Structure thickness in 3D was calculated using the local thickness or sphere-fitting method,[22, 23] and structure model index (an indicator of the relative prevalence of plates and rods) was derived according to the method of Hildebrand and Ruegsegger.[19] Degree of anisotropy was calculated by the mean intercept method.[24] Rendered 3D models were constructed for 3D viewing of trabecular and cortical bone of the analyzed regions as described previously.[25] The image on the right of Figure 6 shows a slice of the studied region color-coded for trabecular thickness.

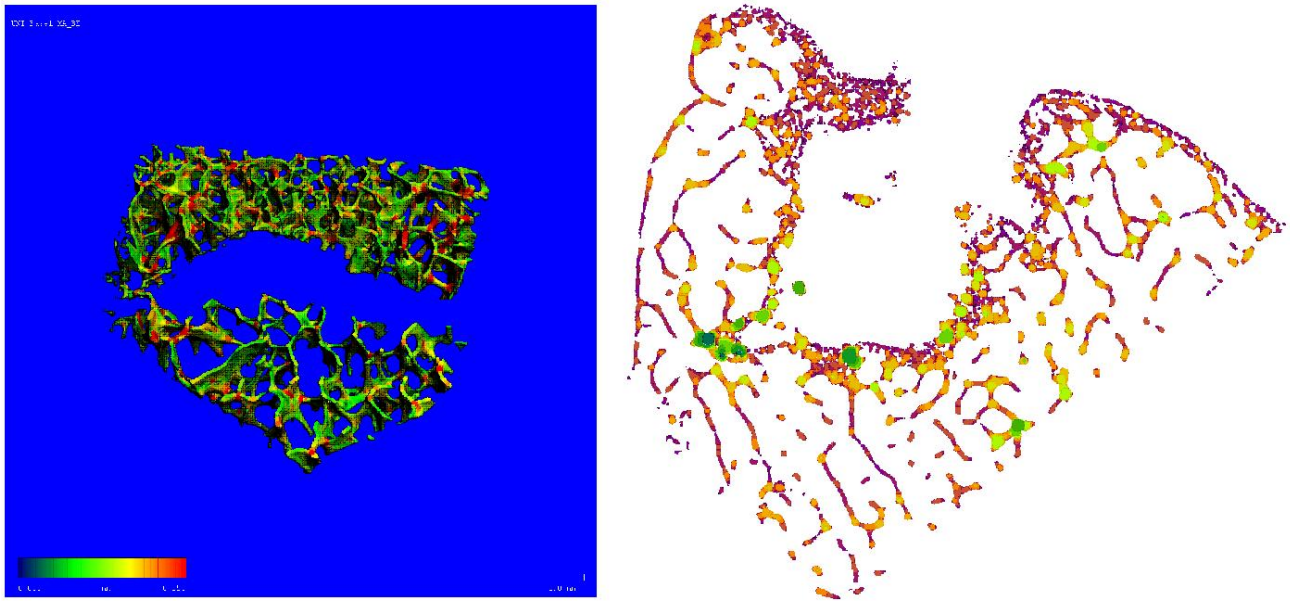

Fig. 6. Color-coded representations of the bony tissue to demonstrate the morphometric analysis.

The quantities extracted from the common volume of the tomographic data are summarized in Table 3. It shows the structure parameters as obtained by the different CT systems and the related software. For BV/TV, Tb.Th and trabecular separation the parameters are quite similar. Significant differences are especially found for the SMI, for the trabecular number and the degree of anisotropy.

Table 3: Structure parameters as determined by Scanco and Skyscan software

	Scanco Medical	Skyscan 1172	Skyscan 1174
Total volume (TV) [mm^3]	28.1	38.1	36.1
Bone volume (BV) [mm^3]	4.4	5.9	6.0
BV/TV [%]	15.7	15.6	16.6
Structure model index (SMI)	0.96	1.77	2.03
Trabecular number (Tb.N*) [1/mm]	2.25	1.41	1.20
Trabecular thickness (Tb. Th*) [mm]	0.09	0.11	0.14
Trabecular separation (Tb. Sp*) [mm]	0.45	0.49	0.51
Degree of anisotropy (DA)	1.3	3.0	3.0

4. DISCUSSION

The vertebral body consists of spongy bone surrounded by the thin compacta. The trabeculae within the vertebral body are mainly directed perpendicular and parallel to the vertebral endplates. The endplates contain a relatively thin layer of sub-chondral bone with an irregularly shaped, porous surface region. Thickness and density of the sub-chondral bone increase towards the periphery. Around the perimeter of the vertebral endplate one finds a bony rim, termed epiphysis anularis. Its central region, covered by a thin cartilaginous layer of hyaline cartilage, forms the interface between the bone and the inter-vertebral disc. Near bone the cartilaginous cells are mostly large surrounded by the partly calcified

extra-cellular matrix. Towards the nucleous pulposus the cells are small and have a flattened morphology. The inter-vertebral disc is composed of a thick ring of fibrous cartilage (annulus fibrosus) that is enveloped by the more gelatinous nucleous pulposus.[26-28]

Although there are some studies comparing the performance of μCT with SRμCT[29] or comparing directly the performances of different μCT-systems,[30] to the best of our knowledge there is no study available that quantitatively compares the density resolution of several μCT-systems with SRμCT using one dedicated specimen. It is really difficult to compare the density resolution or the contrast of conventional μCT-systems, since the photon energy spectrum applied drastically varies and crucially depends on accelerating voltage as well as target and filters used. Therefore, the present communication is based on the two main peaks that served as reference points for half width determination.

In the case of the nanotom® μCT-system the data were recorded during 80 min without additional filter, just using the 400 μm thick Be window. This approach yields the maximum photon intensity and thus the optimum S/N for the selected acquisition time. The drawback of this approach is the presence of some streak artifacts owing to the beam hardening. Hence, segmentation of components, which exhibits similar x-ray absorption, such as the PMMA embedded cartilage become challenging. Introducing a filter to reduce the relative number of photons having low energy, for example Al or Cu, the artifacts are significantly reduced (O. Brunke et al., present proceedings). The better results require, however, a significant increase of the acquisition time.

The recently developed μCT 35™ shows an artifact in the reconstruction center. Its occurrence lies in the reconstruction algorithm of the recorded data. The specimen is acquired stack-wise to better utilize the rather fast fan beam approach. The selected slice is closely located to the transition region between two stacks. The problem can be overcome reducing the stack height, which increases, however, the acquisition time. It should be noted that the μCT 40™ would be the better choice for the presented measurements, because its geometry permits much faster scans and a better S/N ratio. The spatial resolution, that can be achieved by means of the μCT 35™, is improved in comparison to the μCT 40™ .

The Skyscan 1172™ and 1174™ provided rather prominent ring-like artifacts, although the compensation mode was applied. The images presented here, however, are not scaled in the typical manner, where these artifacts are often hardly visible.

Scanco Medical as well as Skyscan offer evaluation software for bone included into the μCT systems. Apart from classic parameters like bone-volume-fraction, trabecular number and trabecular thickness or the SMI, also information can be determined regarding number or volume of pores. The different results of the structure parameters are remarkable especially since both systems rely on similar algorithms known from literature.[17] These differences are difficult to explain and therefore a detailed analysis of a larger specimen such as an entire vertebra body should be performed.

Bernhardt et al.[29] reported that Gaussians could not reasonably fit the histograms of conventional μCT systems. The present paper does not support this experimental result. The disagreement might be related to the specimens used, because the previous study has relied on bony specimens with bulky cuboid titanium implants.

In conclusion, the SRμCT-system with the monochromatic x-ray beam yields the best density resolution and insignificant artifacts that it is the suitable choice for the golden standard comparing the performance of different conventional μCT-systems. The powerful developments in laboratory μCT-technology have led, however, to valuable alternatives to SRμCT for many applications. In particular, the quantitative analysis of bony tissue has become the field for conventional μCT. The main advantage of the conventional μCT-systems with respect to SRμCT is the availability and user friendliness. The systems from Scanco Medical and Skyscan are delivered with advanced analysis software for trabecular bone and are, therefore, extremely supportive in bone research.

REFERENCES

[1] Melloh, M., Roeder, C., Elfering, A., Theis, J.-C., Mueller, U., Staub, L.P., Aghayev, E., Zweig, T., Barz, T., Kohlmann, T., Wieser, S., Juni, P. and Zwahlen, M., "Differences across health care systems in outcome and cost-utility of surgical and conservative treatment of chronic low back pain: a study protocol", BMC Musculoskelet Disord 9 (1), 17 (2008).

[2] Katz, J.N., "Lumbar disc disorders and low back pain: socioeconomic factors and consequences", J Bone Joint Surg Am 88, 3 (2006).

[3] Wenig, C.W., Schmidt, C.O., Kohlmann, T. and Schweikert, T., "Costs of back pain in Germany", Eur J Pain in press (2008).
[4] Hicks, G.E., Fritz, J.M., Delitto, A. and McGill, S.M., "Preliminary development of a clinical prediction rule for determining which patient with low back pain will respond to a stabilization exercise program", Arch Phys Med Rehabil 86, 9 (2005).
[5] Hildebrand, T., Laib, A., Müller, R., Dequeker, J. and Rüegsegger, P., "Direct three-dimensional morphometric analysis of human cancellous bone: microstructural data from spine, femur, iliac crest, and calcaneus,", J Bone Miner Res 14 (7), 7 (1999).
[6] Thurner, P., Beckmann, F. and Müller, B., "An optimization procedure for spatial and density resolution in hard X-ray micro-computed tomography", Nucl. Instrum. Meth. 225 (4), 599-603 (2004).
[7] Beckmann, F., Donath, T., Dose, T., Lippmann, T., Martins, R.V., Metge, J. and Schreyer, A., "Microtomography using synchrotron radiation at DESY: current status and future developments" Proc SPIE 5535, 1-10 (2004).
[8] Müller, B., Beckmann, F., Huser, M., Maspero, F., Székely, G., Ruffieux, K., Thurner, P. and Wintermantel, E., "Non-destructive three-dimensional evaluation of a polymer sponge by micro-tomography using synchrotron radiation ", Biomol Engin 19, 73-78 (2002).
[9] Müller, B., Bernhardt, R., Weitkamp, T., Beckmann, F., Bräuer, R., Schurigt, U., Schrott-Fischer, A., Glueckert, R., Ney, M., Beleites, T., Jolly, C. and Scharnweber, D., "Morphology of bony tissues and implants uncovered by high-resolution tomographic imaging", Int J Mat Res 98 (7), 613-621 (2007).
[10] Kak, A.C. and Slaney, M., [Principles of Computerized Tomographic Imaging], IEEE Press, New York (1988).
[11] Grodzins, L., "Optimum energies for X-ray transmission tomography of small samples", Nucl. Instrum. Meth. 206, S41-S45 (1983).
[12] Feldkamp, L.A., Davis, L.C. and Kress, J.W., "Practical cone-beam algorithm", J Opt Soc Am 1 (6), 7 (1984).
[13] Liu, X. and Sasov, A., [Cluster reconstruction strategies for microCT and nanoCT scanners," in Proceedings of the Fully Three-Dimensional Image Reconstruction Meeting in Radiology and Nuclear Medicine], Fort Douglas / Olympic Village, Salt Lake City, Utah, USA. (2005).
[14] Maes, F., Collignon, A., Vandermeulen, D., Marchal, G. and Suetens, P., [Multi-modality image registration by maximation of mutual information, in Mathematical Methods in Biomedical Image Analysis], pp. 14-22, IEEE (1996).
[15] Viola, P. and Wells, W.M., [Alignment by maximation of mutual information," in Fifth International Conference on Computer Vision] IEEE Computer Society (1995).
[16] Press, W.H., Flannery, B.P., Teukolsky, S.A. and Vetterling, W.T., [Numerical Recipes in C - The Art of Scientific Computing], Cambridge University Press (1988).
[17] Rüegsegger, P., Koller, B. and Müller, R., "A Microtomographic System for the Nondestructive Evaluation of Bone Architecture", Calcif Tissue Int 58, 5 (1996).
[18] Whitehouse, W.J., "The quantitative morphology of anisotropic trabecular bone", J Microscopy 101, 15 (1974).
[19] Hildebrand, T. and Ruegsegger, P., "Quantification of bone microarchitecture with the structure model index.", Comp. Meth. Biomech. Biomed. Eng. 1 8 (1997).
[20] Lorensen, W.E. and Cline, H.E., "Marching cubes: a high resolution 3d surface construction algorithm.", Computer graphics 21 (4), 6 (1987).
[21] Pratt, W.K., Ed., Digital image processing, New York (1991).
[22] Hildebrand, T. and Ruegsegger, P., "A new method for the model independent assessment of thickness in three dimensional images", J. Microsc. 185, 8 (1997).
[23] Remy, E. and Thiel, E., "Medial axis for chamfer distances: computing look-up tables and neighbourhoods in 2D or 3D", Pattern Recognition Letters 23, 12 (2002).
[24] Harrigan, T.P. and Mann, R.W., "Characterisation of microstructural anisotropy in orthotropic materials using a second rank tensor.", J. Mater. Sci. 19, 6 (1984).
[25] Salmon, P.L., Buelens, E. and Sasow, A.Y., "Performance of In Vivo Micro-CT Analysis of Mouse Lumbar Vertebral and Knee Trabecular Bone Architecture", J. Bone Miner. Res 18 (2), (2003).
[26] Rai, P.P., "Intervertebral disc: anatomy-physiology-pathophysiology-treatment", Pain Pract 8 (1), 26 (2008).
[27] Edwards, W.T., Zheng, Y., Ferrara, L.A. and Yuan, H.A., "Structural features and thickness of the vertebral cortex in the thoracolumbar spine", Spine 26 (2), 7 (2001).
[28] Grant, J.P., Oxland, T.R. and Dvorak, M.F., "Mapping the structural properties of the lumbosacral vertebral endplates", Spine 26 (8), 7 (2001).

[29] Bernhardt, R., Scharnweber, D., Müller, B., Thurner, P., Schliephake, H., Wyss, P., Beckmann, F., Goebbels, J. and Worch, H., "Comparison of microfocus- and synchrotron X-ray tomography for the analysis of osteointegration around Ti6Al4V implants", European Cells and Materials 7, 9 (2004).
[30] Sleutel, S., Cnudde, V., Masschaele, B., Vlassenbroek, J., Dierick, M., Van Hoorebeke, L., Jacobs, P. and De Neve, S., "Comparison of different nano- and micro-focus x-ray computed tomography set-ups for the visusalization of the soil microstructure an dsoil organic matter", Comput Geosci 34, 7 (2008).